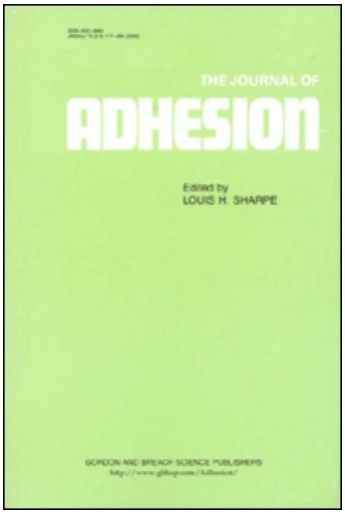


## The Journal of Adhesion

Publication details, including instructions for authors and subscription information:
http://www.informaworld.com/smpp/title~content=t713453635

# Tensile Strength of Single Lap Joint and Scarf Joint between CFRP and Carbon Steel

Chiaki Sato[a]; Kozo Ikegami[a]
[a] Research Laboratory of Precision Machinery and Electronics, Tokyo Institute of Technology, Yokohama, Japan

**To cite this Article** Sato, Chiaki and Ikegami, Kozo(1992) 'Tensile Strength of Single Lap Joint and Scarf Joint between CFRP and Carbon Steel', The Journal of Adhesion, 39: 1, 29 — 41
**To link to this Article: DOI:** 10.1080/00218469208026536
**URL:** http://dx.doi.org/10.1080/00218469208026536

*J. Adhesion*, 1992, Vol. 39, pp. 29–41
Reprints available directly from the publisher
Photocopying permitted by license only

Printed in Great Britain

# Tensile Strength of Single Lap Joint and Scarf Joint between CFRP and Carbon Steel*

CHIAKI SATO and KOZO IKEGAMI

*Research Laboratory of Precision Machinery and Electronics, Tokyo Institute of Technology 4259, Nagatsuta, Midori-Ku, Yokohama 227, Japan*

The strength of single lap joints and scarf joints between carbon cloth laminated plastics (CFRP) and carbon steel bonded with epoxy resin was investigated both analytically and experimentally. The stress and strain distributions under tensile loads of the joints were analyzed by applying the elastic finite element method.

The strength of the joints was predicted by applying the strength law of CFRP, metal, adhesive layer and their interfaces to the calculated stress distributions. The predicted strength was compared with the experimental strength of the joints. The critical positions of the joints and the effects of the overlapped length on the joints were examined.

KEY WORDS single lap joint; scarf joint; CFRP; carbon steel; tensile strength; FEM.



## 1 INTRODUCTION

Fibre reinforced plastics are used in many construction materials, and in many cases bonding is achieved by adhesion. In order to achieve adhesive bonding of high reliability, it is necessary to carry out strength measurements based on stress analysis. In terms of adhesive bonding research, in the past there has been a lot of analytical research into stress distribution within single lap joints by Volkersen,[1] Goland and Reissner,[2] and others, whilst Baker[3] and Amijima[4] have conducted research using the elastic finite element method. In the case of scarf joints too, analytical research has been carried out by Erdogan,[5] Wah,[6] Nagahiro[7] and Hart-Smith,[8] whilst Baker and others have used the elastic finite element method.

As this indicates, much research has been carried out into the stress distribution within joints, but there has been little research into the evaluation of the tensile strength of joints. In this paper we will examine both analytically and experimentally the strength of single lap joints and scarf joints between CFRP and carbon steel.

*Translated from the Japanese and published with the kind permission of The Adhesion Society of Japan. Originally published in *Nihon Setchaku Kyokaishi* [J. Adhesion Soc. Japan] **26**(9), 319–325 (1990).

## 2 STRESS ANALYSIS

### 2.1 Single Lap Joint Configuration

Figure 1 shows the configuration and dimensions of the single lap joint referred to in this paper, and the coordinates used in the analysis. The coordinates used in the analysis are orthogonal coordinates, with the horizontal direction from the centre of the adhesive layer to the surface of the adhesive as the $x$ axis, and the vertical direction to the adhesive surface as the $y$ axis, with the $z$ coordinates at right angles to both of them. The non-dimensional number obtained by dividing the $x$ axis by the length of the adhesive is designated $\overline{X}$, and the tensile load applied to the joint divided by the cross-sectional area of the plane $y$-$z$ of the CFRP adherent body is designated $\sigma_c$. In addition, the value obtained by dividing the thickness of the carbon steel adherent body by the thickness of the CFRP adherent body is designated $\overline{T}$, whilst the length of adhesive $l$ divided by the length of the CFRP adherent body is $\overline{L}$. The width $w$ of the $z$ axis of the joint was set at 25 mm.



### 2.2 Scarf Joint Configuration

Figure 2 shows the configuration, dimensions and coordinates of the scarf joint referred to in this paper. The coordinates used in the analysis are determined in the same way as for the single lap joint, with the $x$ axis extending horizontally from the centre of the adhesive layer, the $y$ axis extending vertically, and the $z$ axis at right angles to both of them. Furthermore, the value obtained by dividing the tensile load applied to the joint by the cross-sectional area of the $y$-$z$ surface of the adherent bodies is designated $\sigma_c$. Length of projection $l$ of the adhesive section across the $x$ axis divided by the thickness of the adherent body is designated $\overline{L}$. The width $w$ of the $z$ axis of the joint was set at 25 mm.

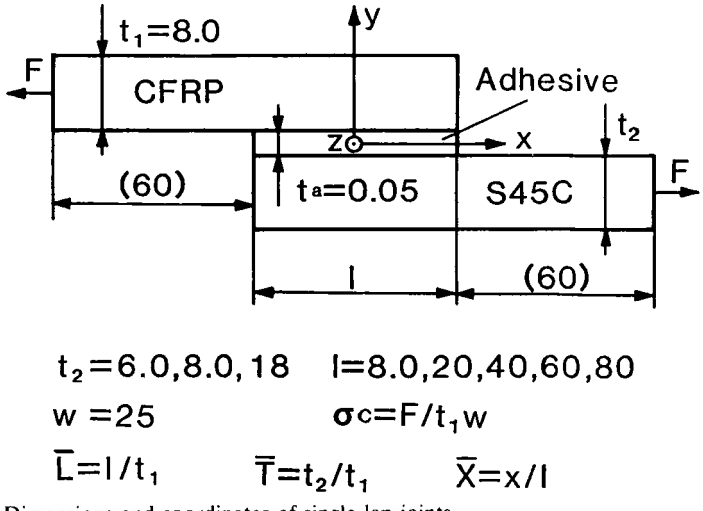


FIGURE 1 Dimensions and coordinates of single lap joints.

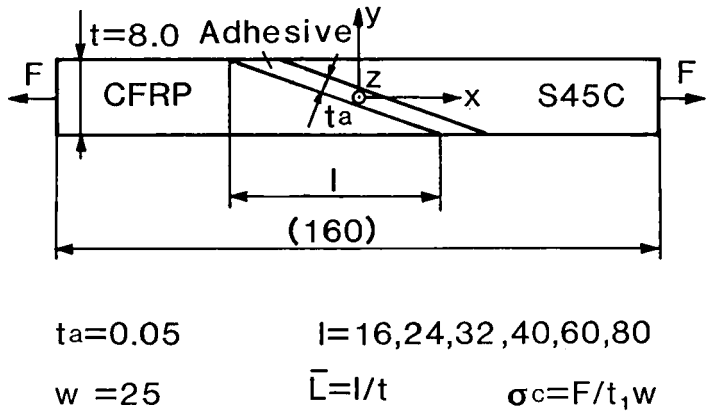


FIGURE 2 Dimensions and coordinates of scarf joints.



### 2.3 Stress Analysis

Stress and strain distribution in single lap joints and scarf joints subjected to tensile shear loading were determined using the elastic finite element method. In this, a planar strain situation was hypothesized, converting the problem to two dimensions and, using a triangular linear element, the calculation was performed within the elastic deformation. The configuration and boundary conditions used in the finite element method are shown for single lap joints in Figure 3, and for scarf joints in Figure 4. In the case of the single lap joint, both adherent bodies were divided into eight layers of thickness, and the adhesive was divided into five layers. Additionally, the area of adhesion covering both adherent bodies and the adhesive was divided vertically into thirty columns. The remaining areas of the adherent bodies were divided into fifteen equal columns. In the case of the scarf joint, both adherent bodies and the adhesive were divided into twenty layers along the $y$ axis. Additionally, both adherent bodies were divided into twenty sections along the $x$ axis, and the adhesive divided into five sections. Table I shows the values of the mechanical properties used in the analysis.

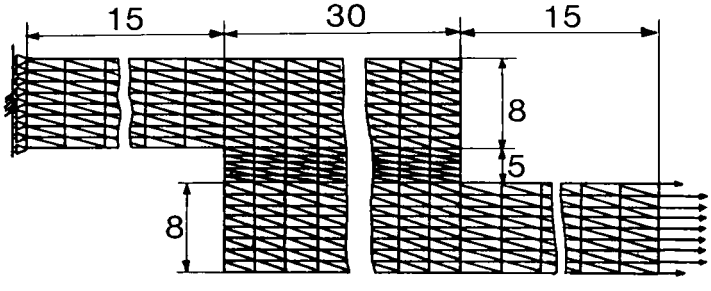


FIGURE 3 Finite element configuration and boundary condition of single lap joint.

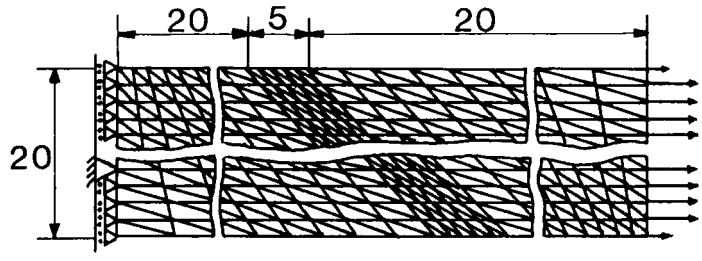


FIGURE 4 Finite element configuration and boundary condition of scarf joint.

TABLE I
Mechanical properties of materials

| | | CFRP | S45C | Adhesive |
|---|---|---|---|---|
| Young's modulus (GPa) | $E_x$<br>$E_y$ | 52.0<br>7.13 | 206 | 3.33 |
| Shear modulus (GPa) | $G_{xy}$<br>$G_{xz}$ | 2.22<br>11.8 | 77.4 | 1.24 |
| Poisson's ratio | $\nu_{xy}$<br>$\nu_{xz}$ | 0.087<br>0.061 | 0.33 | 0.34 |



### 2.4 Strength Evaluation

We applied the strength law to the results obtained using the elastic finite element method and predicted the strength of single lap joint and scarf joint. In this report, we consider that the point at which brittle fractures and yielding first arise within the joint to be initial failure, and the complete separation of the joint to be final failure. As the determining conditions for initial failure, we applied Hoffman's brittleness law[9] to the CFRP adherent body, von Mises' yield conditions to the adhesive and the metal adherent body, and the adhesive strength law[10] to the interface between the metal adherent body and the adhesive. In the case of the interface between the adhesive and the CFRP adherent body, because the matrix of the CFRP adherent body and the material properties of the adhesive are almost identical, the adhesive was considered to be a part of the CFRP adherent body, and their interfacial strength was regarded as being included in the strength of the CFRP adherent body.

For two dimensional problems, Hoffman's brittleness law is represented by the equation:

$$\frac{\sigma_x^2}{F_{tx}F_{cx}}+\frac{\sigma_y^2-\sigma_x\sigma_y}{F_{ty}F_{cy}}+\frac{F_{cx}-F_{tx}}{F_{tx}F_{cx}}\sigma_x+\frac{F_{cy}-F_{ty}}{F_{ty}F_{cy}}\sigma_y+\frac{\tau_{xy}^2}{F_{sxy}}=1 \tag{1}$$

Here, $F_{tx}$ and $F_{ty}$ are respectively the tensile destruction strengths for the $x$ and $y$ directions, $F_{cx}$ and $F_{cy}$ the compression destruction strengths for the $x$ and $y$ directions, and $F_{sxy}$ is the shear destruction strength of the $xy$ surface. These values are shown in Table II.

TABLE II
Parameters of failure criteria

| | | CFRP | S45C | Adhesive |
|---|---|---|---|---|
| Tensile strength (MPa) | $F_{tx}$ | 289 | 343 | 64.0 |
| | $F_{ty}$ | 24.1 | | |
| Compressive strength (MPa) | $F_{cx}$ | 326 | | |
| | $F_{cy}$ | 350 | | |
| Shear strength (MPa) | $F_{sxy}$ | 37.6 | 200 | 37.0 |
| | $F_{sxz}$ | — | | |
| Interfacial strength (MPa) | $F_n$ | — | 31.5 | — |
| | $F_s$ | — | 38.0 | — |
| | m | — | 8.66 | — |

Von Mises' yield conditions applied to adhesive and the metal adherent body are shown by the following equation:

$$(\sigma_x^2 - \sigma_x\sigma_y + \sigma_y^2 + 3\,\tau_{xy}^2)^{1/2} / F_{oi} = 1 \tag{2}$$

Here, $F_{oi}$ is the tensile or compressive yield stress, and the values for carbon steel and adhesive are shown in Table II.

Furthermore, the interfacial strength law is shown by the following equation:

$$\left|\frac{\sigma_n}{F_n}\right|^m + \left|\frac{\tau_s}{F_s}\right|^m = 1 \tag{3}$$

Here, $F_n$ is the tensile strength of the adhesive surface perpendicular to the interface, $F_s$ is the shear strength of the adhesive surface parallel to the interface, and $m$ is the experimentally determined coefficient. These values are shown in Table II.



## 3 EXPERIMENTAL METHOD

### 3.1 Test Strips

In the experiments, the same type of material was used as the CFRP adherent body test strips for the single lap joint and the scarf joint. These were made using carbon cross built up in layers in a metal mould using the hand lay up method, with TORAYCA T-300 (TORAY) used in the carbon cross, and the room-temperature-hardening vinyl ester resin RIPOXY R-802 (Showa Polymer) used in the matrix. In every layer the direction of the fibres was laid out parallel to the $x$ and $y$ axes. Thirty layers were used.The carbon steel adherent body was made from a polished bar of S45C. The adhesive used was Scotch-Weld 1838 (Sumitomo-3M).

The surface of the carbon steel adherent body was prepared by grinding, then finishing with #600 sandpaper. In order to remove any mould-releasing agent, the surface of the CFRP adherent body used in the single lap joint was prepared by polishing with #600 sandpaper. In the case of the CFRP adherent body used in the scarf joint, because the adherent surface was shaped by cutting, there was no risk

of influence from mould-releasing agents, so the sandpaper treatment was not carried out. After this, the adherent surfaces were washed with acetone, and adhesion was effected. Finally, curing was carried out at 65°C for 120 minutes.

### 3.2 Strength Testing of Joints

Tensile loading was applied to both single lap joints and scarf joints at room temperature by means of a tensile strength test machine, and the failure strength of the joints was measured. In order to detect the deformation behaviour of the joint under load, a single axis strain gauge was positioned as shown in Figure 5. The strain gauge was set to measure strain along the $x$ axis. The readout of this gauge was recorded as well as the load applied to the joint. With the onset of initial failure within the joint, there is a re-distribution of stress resulting from plastic deformation or crack development, and at this point the stress-strain curve on the stress-strain graph deviates from a straight line. In this report, we take this point where the stress-strain curve loses its straightness as initial failure, and the separation of the joint into two or more sections, when load ceases to be conveyed through the joint, as final failure. Figure 6 shows a typical stress-strain curve.

## 4 COMPARISON WITH EXPERIMENT

### 4.1 Strength of Single Lap Joint

The strength laws for adherent bodies, adhesive and adhesion interface were applied to the stress distribution within the joint, and the applied stress at the respective

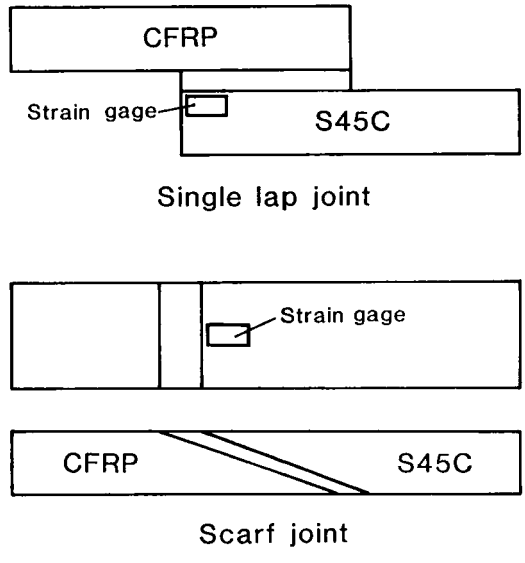


FIGURE 5 Position of strain gage.

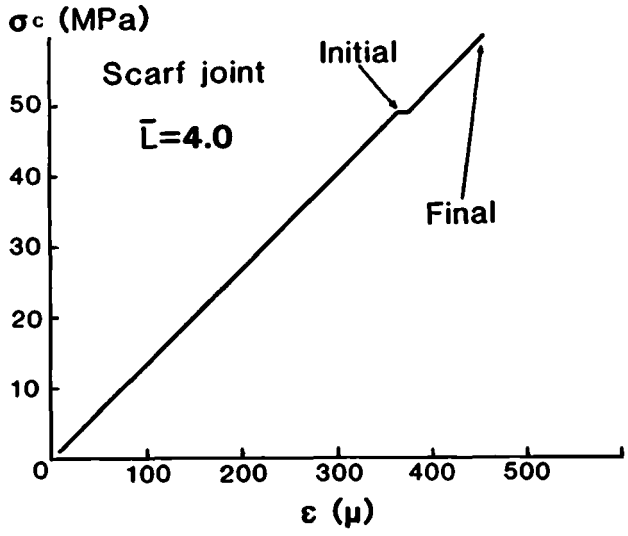


FIGURE 6 Typical stress-strain curve of scarf joint.



positions at the point of initial failure was calculated. Figure 7 shows the values $\sigma_c$ of the applied stress at the various positions at the point of initial failure for a single lap joint where $\overline{T}=1.0$, $\overline{L}=5.0$. In this joint, the lowest strength sections of the interface, adhesive and CFRP are concentrated in the vicinity of the left-hand edge of the adhesive layer. Conversely, the lowest strength section of the carbon steel adherent body is near the right-hand edge of the adhesive layer. Additionally, the left edge of the adhesion interface has the lowest strength of the whole joint. It is thought that the strength of this section governs the initial failure strength of the joint. The same tendency can be seen in other single lap joints.

The changes in initial failure strengths of adhesive and interface of the bonded materials in single lap joints in relation to length $\overline{L}$ are shown in Figure 8 ($\overline{T}=0.75$),

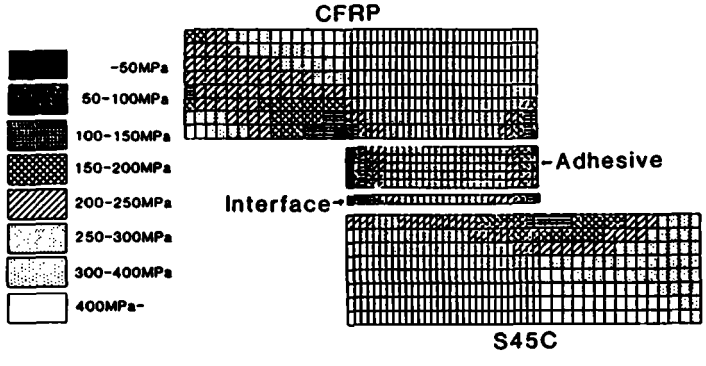


FIGURE 7 Distribution of calculated failure strength in single lap joint ($\overline{T}=1.0$, $\overline{L}=5.0$)

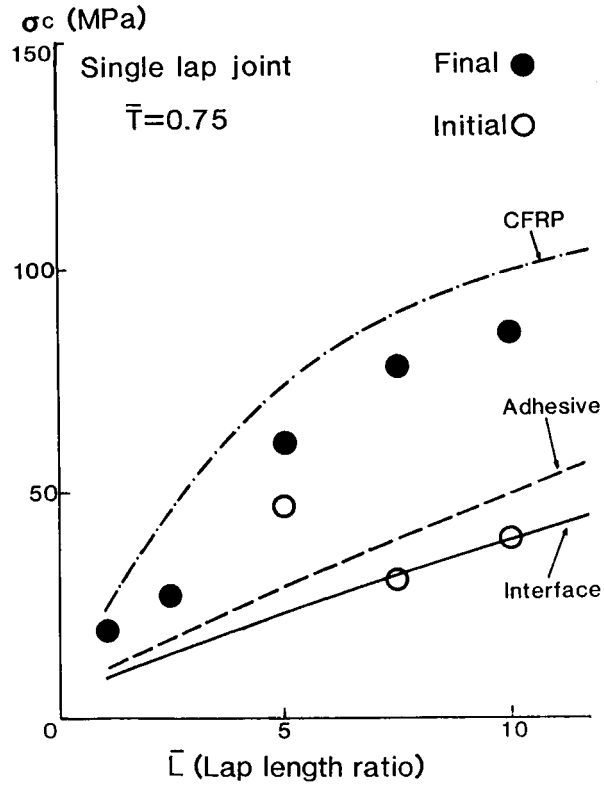


FIGURE 8 Variation of calculated and experimental failure strength in single lap joint ($\bar{T}=0.75$) with lap length ratio $\bar{L}$.

Figure 10 ($\bar{T}=1.0$) and Figure 11 ($\bar{T}=2.25$). The failure strength of the metal adherent body is much greater than that of the other parts, so it is not shown in the diagrams. In every case, in the range $\bar{L}\leq 10$, the strength of the adhesion interface is lowest, with strengths increasing in the order of adhesive, CFRP adherent body, and carbon steel adherent body. Furthermore, in this instance the strength of the adhesion interface increases in direct proportion to $\bar{L}$. Moreover, as $\bar{T}$ increases, which is to say as the thickness of the carbon steel adherent body increases, the strength of the adhesion interface decreases. Here, the smallest values for initial failure strength for adherent bodies, adhesive, and adhesion interface represent the load which brings about initial failure in the joint.

Figures 8 to 10 show the failure strengths obtained experimentally. In each joint where $\bar{T}=2.25$ there is close agreement between the values for initial failure strength obtained experimentally and those obtained by calculation, but in areas where $\bar{L}\geq 5.0$ for joints where $\bar{T}=0.75$, and in areas where $\bar{L}\leq 5.0$ for joints where $\bar{T}=1.0$, the experimental values for failure strength are greater than the calculated values.

In single lap joints when the failure strength is calculated by the method used in this report, the calculated failure strength in cases where $\bar{T}$ is less than 1 tends to

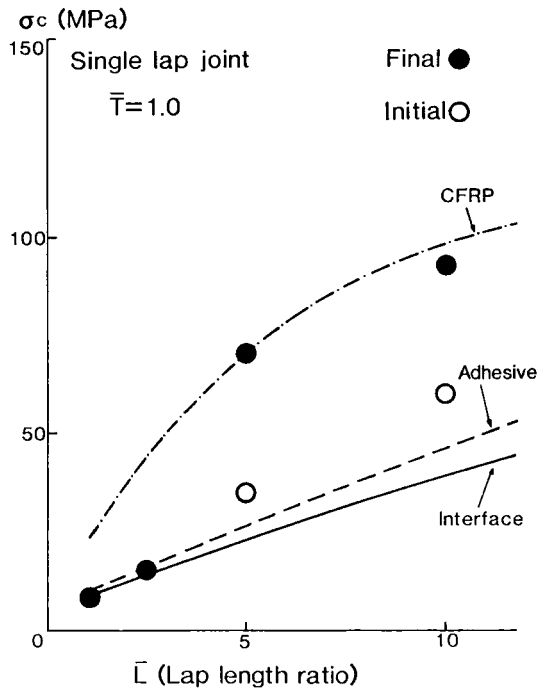


FIGURE 9 Variation of calculated and experimental failure strength in single lap joint ($\bar{T}=1.0$) with lap length ratio $\bar{L}$.

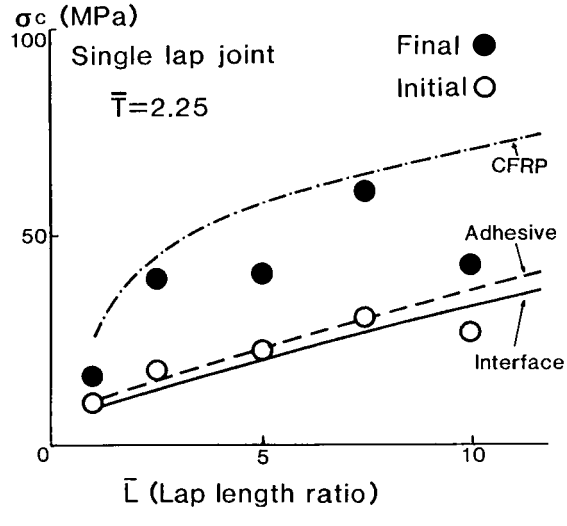


FIGURE 10 Variation of calculated and experimental failure strength in single lap joint ($\bar{T}=2.25$) with lap length ratio $\bar{L}$.

be greater than the true failure strength. However, as $\overline{T}$ gets larger and the rigidity of the carbon steel adherent body greatly exceeds the rigidity of the CFRP adherent body, the experimental values and calculated values show close agreement.

### 4.2 Scarf Joint Strength

Figure 11 shows the failure strength distribution in a scarf joint where $\overline{L} = 5.0$. Here the lowest strength section is the adhesive layer and adhesion interface near the sharp edge of the carbon steel adherent body, and it is predicted that this is where initial failure of the joint will occur. The same tendency is seen in other scarf joints.

Figure 12 shows the variation in failure strength in relation to $\overline{L}$ for all sections. The failure strengths for adhesive, interface and CFRP shown here are all values for positions near the sharp edge of the carbon steel adherent body. As this figure shows, initial failure when $\overline{L}$ is small is predicted to occur in the interface.

Figure 12 shows the initial failure and final failure strengths obtained experimentally. When $\overline{L}$ is between 2 and 4, the experimental values for initial failure strength agree closely with the calculated figures, but when $\overline{L} = 5$ the experimental figures are greater than the calculated values, and when $\overline{L} = 10$ the experimental values are once again greater than the calculated values.



### 4.3 Comparison of Joint Strength

Figure 13 shows the comparison between failure strengths for single lap joints where $\overline{T} = 1.0$ where the CFRP adherent body and carbon steel adherent body are of equal thickness, and a scarf joint of equivalent thickness. Usually, the calculated failure strength of the scarf joint is greater, regardless of the value of $\overline{L}$. In particular, when $\overline{L}$ is less than 5, this tendency is striking. However, the rate of increase in strength in relation to $\overline{L}$ is not much different between single lap joints and scarf joints when $\overline{L}$ exceeds 3.

When we examine the results of the strength experiments (Figures 9 and 11), when $\overline{L}$ is less than 5 the failure strength of scarf joints as predicted exceeds that of

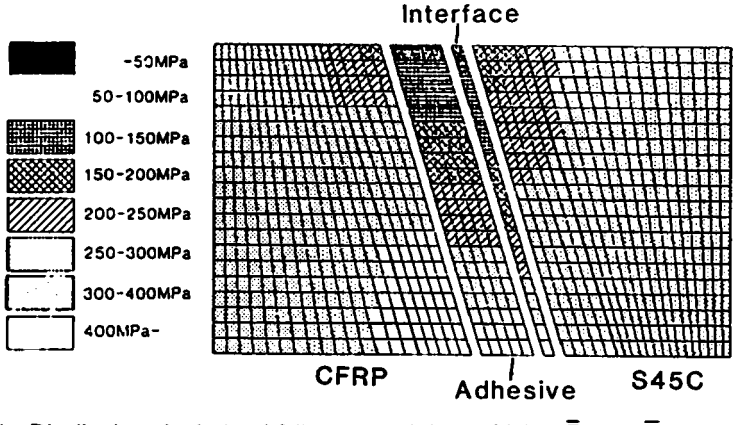


FIGURE 11 Distribution of calculated failure strength in scarf joint ($\overline{T} = 1.0$, $\overline{L} = 5.0$).

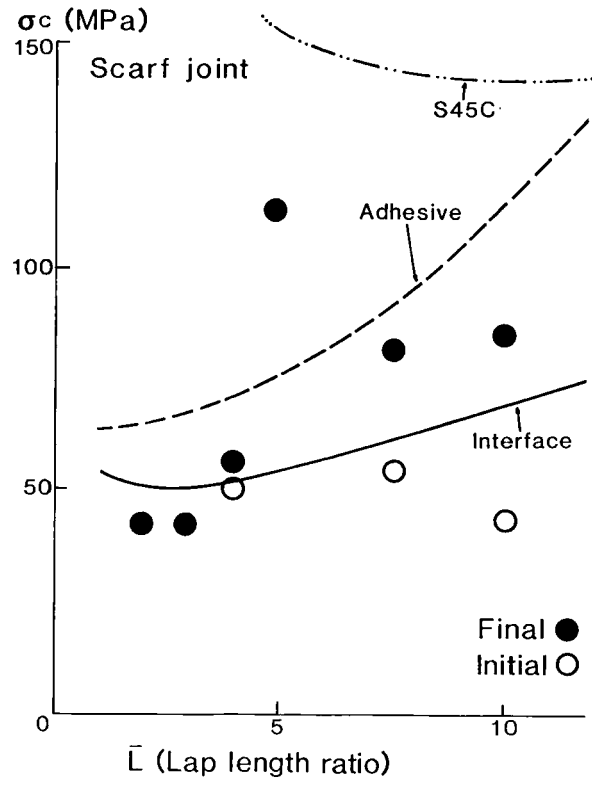


FIGURE 12 Variation of calculated and experimental failure strength in scarf joint with lap length ratio $\bar{L}$.

single lap joints. However, when $\bar{L}$ is around 10, the failure strength of single lap joints exceeds that of scarf joints.

When bonding materials are of different types because the physical properties of the two adherent bodies are dissimilar, if a load is applied suddenly it is easy for concentrations of stress to occur. For this reason, scarf joints are often used because of their ability to transfer load gradually. In the CFRP-carbon steel joints studied in this report too, scarf joints had fewer concentrations of stress than single lap joints for the same values of $\bar{L}$. Accordingly, predicted failure strengths for scarf joints are greater. However, for values of $\bar{L}$ around 10, real failure strength values for single lap joints are greater than those for scarf joints. In scarf joints, when $\bar{L}$ exceeds 5, experimental failure strengths fall below the calculated failure strengths. Furthermore, in this situation failure is predicted to occur in the adhesion interface but, in fact, complex failure is observed in the CFRP and adhesive, as well as in the interface. This is thought to be due to the fact that as $\bar{L}$ is increased, the load which gives rise to failure in the adhesive and the CFRP nearby decreases. However, as the length of the adhesive section increases, the load giving rise to failure in the adhesive itself increases. Accordingly, it may be that the reason that complex failure occurs is that the load giving rise to failure in the CFRP decreases.

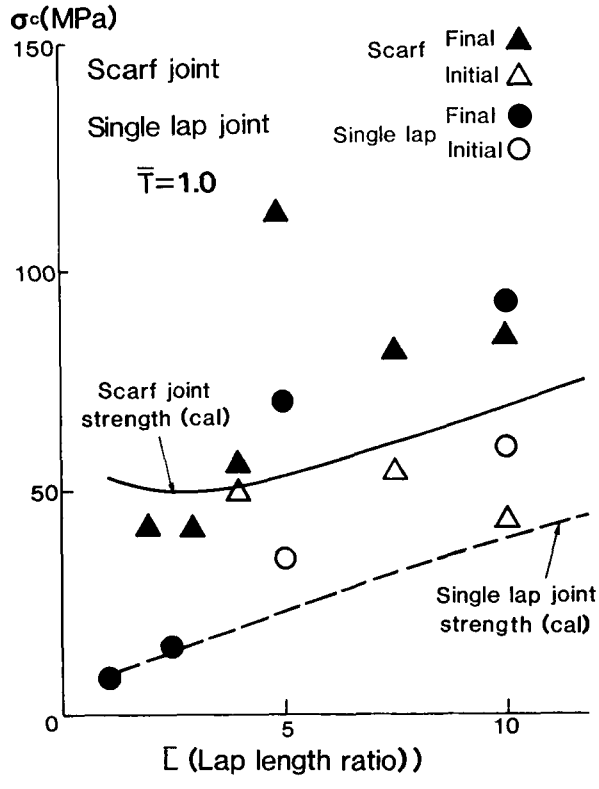


FIGURE 13 Comparison of the strength between single lap joints and scarf joints.

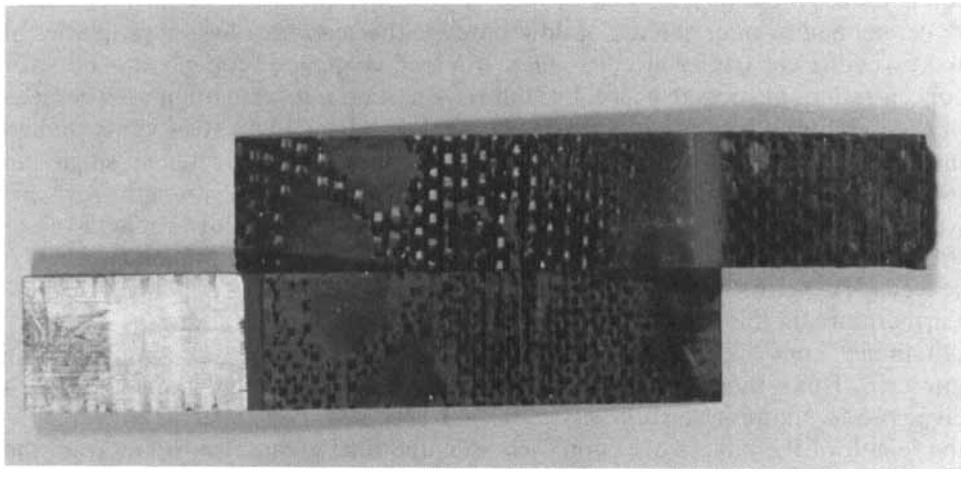

PHOTOGRAPH 1 Fractured surface of scarf joint.

If we examine the sections in which complex failure occurs, as Photograph 1 shows, the fibres in the CFRP aligned along the $z$ axis are drawn out and stuck to the adhesive. Within the ranges covered in the current experiments, this tendency becomes more striking as the value of $\overline{L}$ increases. It may be that the load required to draw out the fibres running in the same direction as the direction of load is smaller than that required to break the fibres running parallel to the direction of load. Thus, it is considered that as $\overline{L}$ increases and the phenomenon of the fibres being pulled out becomes more marked, the micro strength of the CFRP section becomes less than the CFRP macro strength calculated using Hoffman's brittleness law. This is thought to be the reason behind the decrease in the failure strength of the scarf joint.

## 5 CONCLUSION

In this report we have examined both experimentally and theoretically the failure strengths under tensile loading of single lap joints and scarf joints between CFRP and carbon steel (S45C). First, stress and strain distribution within the joints were analysed using the elastic finite element method, and then these results were confirmed experimentally. Additionally, the strength law was applied to the calculated results, the joints' failure strengths were calculated, and these results were compared with the experimental results.

The following is a summary of the results contained in this report:

1. It is generally possible to predict the failure strength of single lap joints by applying the strength law to the stress analysis result obtained by the elastic finite element method.
2. For the ranges covered in the current experiments, for single lap joints, the failure strength increases in direct proportion to the lap length.
3. For single lap joints of the same lap length, the failure strength decreases as the thickness of the carbon steel adherent body increases in comparison to the thickness of the CFRP adherent body.
4. In the case of scarf joint failure strength, as the length of lap increases, drawing out of the fibres in the CFRP adherent body occurs, and failure occurs at loads less than the predicted strengths.
5. For both single lap joints and scarf joints, there is little difference in failure strengths when lap length becomes large.



## References

1. O. Volkersen, *Luftfahrtforschung* **15,** 41 (1938).
2. M. Goland and E. Reissner, *J. Applied Mechanics* **11,** A17 (1944).
3. R. M. Baker and F. Hatt, *AIAAJ.* **16,** 204 (1978).
4. S. Amijima *et al., J. Adhesion Society of Japan* **19,** 175 (1983).
5. F. Erdogan and M. Raywani, *J. Composite Materials* **5,** 378 (1971).
6. T. Wah, *Int. J. Solids Structures* **12,** 491 (1976).
7. T. Nagahiro, *et al., J. Adhesion Society of Japan* **17,** 499 (1981).
8. L. J. Hart-Smith, NASA CR 112237, Jan (1973).
9. T. Hayashi, *Composite Materials Engineering* (Nikka Giren, 1977).
10. T. Sugibayashi and K. Ikegami, *J. Adhesion Society of Japan* **18,** 102 (1982).